Predominant Conformations of (2*R*,3*R*)-(−)-2,3-Butanediol

Feng Wang and P. L. Polavarapu*

Department of Chemistry, Vanderbilt University, Nashville, TN37235

Received: February 12, 2001; In Final Form: May 14, 2001

Vibrational absorption and circular dichroism spectra of (−)-2,3-butanediol have been measured in CS_2 and CCl_4 solutions in the 2000−900 cm^{-1} region. Experimental spectra obtained at different concentrations are compared with the ab initio predictions of absorption and circular dichroism spectra obtained with density functional theory using the B3LYP/6-31G* basis set for different conformers of (2*R*,3*R*)-2,3-butanediol. The Boltzmann populations, obtained from Gibbs free energies, indicate the presence of 10 predominant conformations for isolated molecules. The conformational stability of (2*R*,3*R*)-(−)-2,3-butanediol in dilute solution is also investigated on the basis of calculations with self-consistent reaction field (SCRF) methods. The population-weighted theoretical spectra are in satisfactory agreement with the experimental spectra obtained at dilute concentrations. Intramolecular hydrogen bonding in (2*R*,3*R*)-(−)-2,3-butanediol is observed in the dilute solution, and intermolecular hydrogen bonding is evident in the experimental spectra at higher concentrations. Solvent influence on the absorption and circular dichroism spectra is also presented.

Introduction

The absolute configuration and predominant conformations of (2*R*,3*R*)-(−)-2,3-butanediol are particularly important in stereochemical relationships since the stereochemistry of a large number of compounds have been related to that of (2*R*,3*R*)-(−)-2,3-butanediol and its derivatives[1]. The absolute configuration of chiral 2,3-butanediol was determined by chemical correlation[2], and (+)-2,3-butanediol was assigned an (*2S*,*3S*) configuration on the basis of chemical correlation with (2*R*,3*R*)-(+)-tartaric acid. Recently, the conformational preferences of chiral (2*R*,3*R*)-(−)-2,3-butanediol also became an important subject since (2*R*,3*R*)-2,3-butanediol has been used as a model to investigate the methyl ester of (*R*,*R*)-tartaric acid monoamide[3]. However, there are only limited experimental data available on the conformational properties of 2,3-butanediol. Gallwey et al.[4a] have measured the ^1H NMR spectra to investigate the conformation of (2*R*,3*R*)-2,3-butanediol. They concluded that the G^- conformation (See Figure 1 for conformation labels) has the lowest energy and that there is almost 84−90% of the G^- conformer in nonpolar solvent, CCl_4. As the solvent changes from low polar through protic to very polar aprotic, the G^- conformation decreases, and the *T* conformation increases, while the G^+ conformation is constant at 6−20%. No information was available on the orientation of C−C−O−H segment. In another proton NMR investigation,[4b] in dilute CCl_4 solution, the population of G^- conformation is suggested as 51%, and the combined population of G^+ and *T* was suggested as 49%. Although some information on C−C−O−H segment was also given here, the studied conformations are only a small part of the total 27 conformations that one would obtain when rotations of three dihedral angles H_A−O−C−C, O−C−C−O, and C−C−O−H_B (See Figure 1) are considered. These authors[4b] considered (g^+G^-t'), ($g^+G^-g'^-$), (g^-G^+t'), and ($g^-G^+g'^+$) conformations for the analysis of their experimental data. ^{13}C NMR studies[5] and molecular mechanics[6] also deduced the decrease of gauche form and increase of trans form (for the O−C−C−O segment) as the solvent changed from apolar to polar.

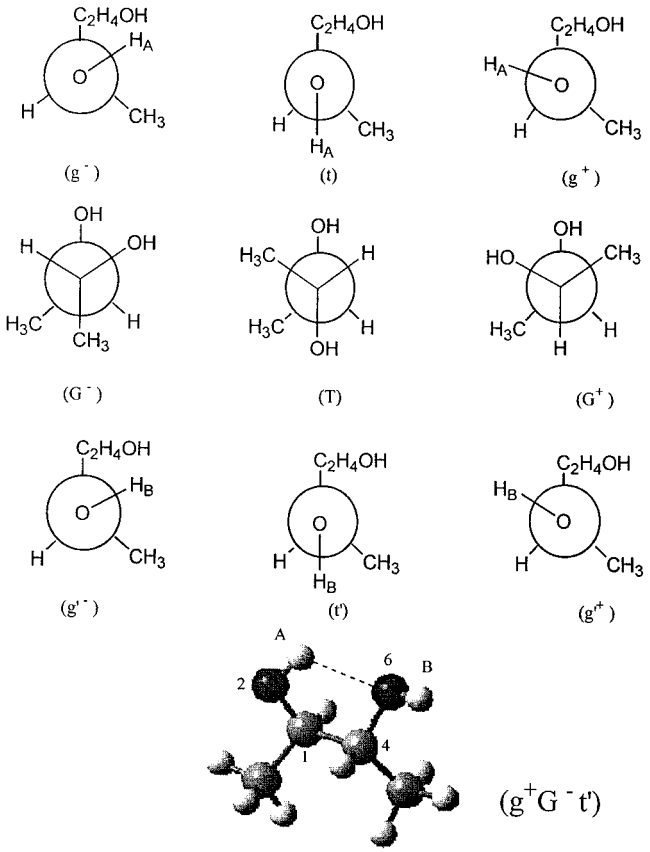

Figure 1. Different conformations of (2*R*,3*R*)-(−)-2,3-butanediol, based on the differences in the dihedral angles $C_4-C_1-O_2-H_A$ (labeled as g^+, t, and g^-), $O_2-C_1-C_4-O_6$ (labeled as T, G^+, and G^-), and $C_1-C_4-O_6-H_B$ (labeled as t′, g'^+, and g'^-). The bottom structure is intended for defining two types of COH groups: $C_1O_2H_A$ as type A, where the OH group is locked in intramolecular hydrogen bonding; $C_4O_6H_B$ as type B, where the OH group is free to participate in intermolecular hydrogen bonding.

In recent years, the experimental and ab initio vibrational optical activity (VOA) spectra are combined to determine the

10.1021/jp010550z CCC: $20.00
Published on Web 06/21/2001

absolute configuration and predominant conformations of chiral molecules in the solution phase.[7−8] Vibrational circular dichroism (VCD) and vibrational Raman optical activity (VROA) are two different branches of VOA. The following developments make the utility of VCD a reliable tool for structural elucidation: (a) VCD instrumentation has been improved to obtain the VCD spectra with enhanced signal-to-noise ratio; (b) density functional theory (DFT)[9] is used, which makes ab initio applications state-of-the-art. The DFT theory provides vibrational frequencies and intensities that are comparable to the post-SCF calculations employing electron correlation and has also been extended to the VCD intensity calculations[10] and implemented in standard software.[11] These advances make it possible to use VCD for a reliable determination of the absolute configuration and predominant conformations in the solution phase.

Vibrational absorption and vibrational circular dichroism (VCD) spectra at 0.0099 M in CCl_4 solution of (2*R*,3*R*)-2,3-butanediol have also been undertaken in the OH stretching region,[4b] but corresponding ab initio calculations could not be undertaken at that time. VROA of (−)-2,3-butanediol has been reported,[12] and it was suggested that all three conformers (G^+, T, and G^-) might be present with the possibility that G^- might be dominant. The absolute configuration of 2,3-butanediol has not yet been confirmed by spectroscopic techniques; moreover, only limited information is available on the predominant conformations of 2,3-butanediol in solution phase. It is useful to have the experimental and theoretical data that would identify the absolute configuration of, and predominant conformations preferred by, 2,3-butanediol.

Interactions between molecules have significant influence on the conformational stability of molecules participating in intermolecular hydrogen bonding, dipole−dipole interactions, and dipole-induced dipole interactions.[13−14] The influence of concentration and solvent on the conformational stability of 2-butanol,[13a] 3-butyn-2-ol,[13b] and (S)-(+)-epichlorohydrin[14] has been studied recently. Unlike in 2-butanol, 3-butyn-2-ol, and (S)-(+)-epichlorohydrin, there is intramolecular hydrogen bonding in some conformations of chiral 2,3-butanediol. The changes in vibrational absorption and VCD spectra with concentration, in general, may come from (a) the influence of intermolecular interactions (such as hydrogen bonding, dipole−dipole interaction, and dipole-induced dipole interaction) on the relative conformation populations, which results in the population-weighted spectra to be different, and (b) the influence of intermolecular interactions on structural parameters and, hence, on force constants in different conformations. In the case of chiral (2*R*,3*R*)-(−)-2,3-butanediol, it is not clear if either one or both of these two sources prevail and result in variations in absorption and VCD spectra as a function of concentration. Vibrational absorption and VCD spectra of (2*R*,3*R*)-(−)-2,3-butanediol are investigated here to determine its absolute configuration, equilibrium composition of conformers in dilute solutions, and the influence of intermolecular interactions on conformer compositions.

Procedures

(2*R*,3*R*)-(−)-2,3-butanediol was purchased from Aldrich Chemical Co. The infrared and VCD spectra were recorded on a commercial Fourier transform VCD spectrometer, Chiralir (Bomem-BioTools, Canada) with a ZnSe beam splitter, BaF_2 polarizer, optical filter (transmitting below 2000 cm^{-1}), and a 2×2 mm^2 HgCdTe detector. One difference from the standard Chiralir instrument is that the photoelastic modulator used was a PEM-80 model (Hinds Instruments) without AR coating on the ZnSe optical element. The VCD spectra were recorded, using the supplied Chiralir software, with 3 h data collection time at 4 cm^{-1} resolution. The transmission properties of optical filter and BaF_2 substrates used in the instrument restrict the range of measurements to 2000−900 cm^{-1}. Spectra were measured in CS_2 and CCl_4 solvents at four different concentrations, 0.01, 0.05, 0.077, and 0.315 M at path lengths of ∼1560, ∼360, ∼300, and ∼80 μm, respectively. In addition, spectra were also recorded in CH_2Cl_2 at ∼0.05 M at a path length of ∼300 μm. The sample was held in a variable path length cell with BaF_2 windows. In the presented absorption spectra, the solvent absorption was subtracted out. In the presented VCD spectra, the raw VCD spectrum of the solvent was subtracted. Spectra of the neat liquid were also measured, and the sample was held in a fixed path length cell (6 μm) with BaF_2 windows.

The ab initio vibrational frequencies, absorption, and VCD intensities for (2*R*,3*R*)-(−)-2,3-butanediol were calculated using Gaussian 98 program[11] on a Pentium II 300 MHz PC. The calculations used the density functional theory (DFT) with the B3LYP functional[9,15] and the 6-31G* basis set.[16] The procedure for calculating the VCD intensities using DFT theory is due to Cheeseman et al.,[10] as implemented in Gaussian 98 program.[11] The theoretical absorption and VCD spectra were simulated with Lorentzian band shapes and 8 cm^{-1} full width at half-height. Since the ab initio predicted band positions are higher than the experimental values, the ab initio frequencies have been scaled with 0.96.

For the normal coordinate analysis, the following procedure has been used to transform the ab initio results into the form required for our normal coordinate analysis programs. The Cartesian coordinates obtained for the optimized structure were input into the G-matrix program[17] together with the definitions of 42 internal coordinates. The B-matrix obtained in the output was then used to convert the ab initio force field in Cartesian coordinates to a force field in the internal coordinates. The force constants were then input along with the B-matrix into the vibrational optical activity program developed in our laboratory to calculate the potential energy distribution (PED) for all 10 predominant conformers.

Results and Discussion

Twenty-seven possible conformations of (2*R*,3*R*)-(−)-2,3-butanediol (see Figure 1), differing in the dihedral angle $C_4-C_1-O_2-H_A$ (labeled as g^+, t, and g^-), $O_2-C_1-C_4-O_6$ (labeled as G^+, T, and G^-), and $C_1-C_4-O_6-H_B$ (labeled at g'^+, t′, and g'^-), are investigated. The geometries were optimized with the B3LYP/6-31G* basis set. Of the 27 conformations, 11 conformations had very high energies or did not converge. The converged $C_4-C_1-O_2-H_A$, $O_2-C_1-C_4-O_6$, and $C_1-C_4-O_6-H_B$ dihedral angles, optimized energies, and relative populations based on the Gibbs free energies for the remaining 16 conformations are listed in Table 1. Because of symmetry, only 10 out of these 16 conformations are unique (for example, $g^-G^-g'^+$ and $g^+G^-g'^-$ are equivalent). The gauche $O_2-C_1-C_4-O_6$ conformations are more stable than trans $O_2-C_1-C_4-O_6$ conformations for isolated molecules because it is not possible to form intramolecular hydrogen bonds in the trans $O_2-C_1-C_4-O_6$ conformation. For similar reasons, $g^+G^+g'^+$ and g^+G^+t' are not as stable as $g^+G^+g'^-$, and $g^-G^-g'^-$ and g^-G^-t' are not as stable as $g^-G^-g'^+$. The Gibbs energy differences among the most stable gauche $O_2-C_1-C_4-O_6$ conformations are not very large, so none of the most stable gauche $O_2-C_1-C_4-O_6$ conformations (listed in Table 1) can be neglected. The

TABLE 1: Conformations and Energies of (2*R*,3*R*)-2,3-butanediol

	starting geom.[b]			converged geom.[b]			energy[c]				dipole
label[a]	$C_4C_1O_2H_A$	$O_2C_1C_4O_6$	$C_1C_4O_6H_B$	$C_4C_1O_2H_A$	$O_2C_1C_4O_6$	$C_1C_4O_6H_B$	electronic	gibbs	ΔE[d]	pop.[e]	moment
1 ($g^-G^-g'^+$)	−60	−60	60	−74.5	−49.2	36.8	−308.880213	−308.768698	0.000	0.169	2.4926
2 ($g^+G^-g'^-$)	60	−60	−60	36.8	−49.2	−74.6	−308.880213	−308.768698	0.000	0.169	2.4926
3 ($tG^-g'^+$)	180	−60	60	166.0	−54.0	44.0	−308.879665	−308.768535	0.101	0.142	2.6598
4 (g^+G^-t')	60	−60	180	44.0	−54.0	165.8	−308.879665	−308.768535	0.101	0.142	2.6598
5 (g^-G^+t')	−60	60	180	−48.7	57.1	−166.9	−308.879338	−308.768015	0.429	0.082	2.4744
6 ($tG^+g'^-$)	180	60	−60	−167.1	57.1	−48.7	−308.879338	−308.768015	0.429	0.082	2.4744
7 ($g^+G^-g'^+$)	60	−60	60	71.2	−43.5	71.4	−308.877846	−308.767673	0.643	0.057	0.4384
8 ($g^-G^+g'^+$)	−60	60	60	−41.1	52.7	74.2	−308.879075	−308.767571	0.707	0.051	2.3513
9 ($g^+G^+g'^-$)	60	60	−60	74.2	52.7	−41.2	−308.879075	−308.767571	0.707	0.051	2.3513
10 ($g^-G^+g'^-$)	−60	60	−60	−76.4	52.6	−76.4	−308.877941	−308.767544	0.724	0.050	0.2588
11 (tTt')	180	180	180	−179.0	−172.3	−179.0	−308.874561	−308.763949	2.980	0.001	0.3084
12 (g^+Tt')	60	180	180	64.3	−172.7	−176.1	−308.874502	−308.763781	3.085	0.001	2.0844
13 (tTg'^+)	180	180	60	−176.1	−172.7	64.3	−308.874502	−308.763781	3.085	0.001	2.0844
14 ($g^+Tg'^+$)	60	180	60	58.2	−175.0	58.2	−308.874461	−308.763655	3.165	0.001	1.9978
15 ($g^-Tg'^+$)	−60	180	60	−78.0	−171.7	62.9	−308.874449	−308.763651	3.167	0.001	0.3764
16 ($g^+Tg'^-$)	60	180	−60	62.8	−171.7	−78.0	−308.874449	−308.763651	3.167	0.001	0.3764
17 (g^-Tt')	−60	180	180	−81.5	−172.1	175.9	−308.874146				
18 (tTg'^-)	180	180	−60	175.9	−172.1	−81.6	−308.874146				
19 ($g^-Tg'^-$)	−60	180	−60	−76.7	−170.0	−76.7	−308.873592				
20 (tG^+t')	180	60	180	−174.3	71.9	−174.2	−308.872509				
21 ($tG^+g'^+$)	180	60	60	179.3	68.2	64.8	−308.872110				
22 (g^+G^+t')	60	60	180	65.0	68.3	179.2	−308.872110				
23 (tG^-t')	180	−60	180	169.5	−66.9	169.4	−308.870798				
24 ($g^-G^-g'^-$)	−60	−60	−60	converged to ($g^+G^-g'^-$)							
25 (g^-G^-t')	−60	−60	180	converged to (g^+G^-t')							
26 ($tG^-g'^-$)	180	−60	−60	converged to ($tG^-g'^+$)							
27 ($g^+G^+g'^+$)	60	60	60	converged to (g^-G^+t')							

[a] See Figure 1 for the labels. [b] Dihedral angle. [c] In Hartrees. [d] Relative energy difference, in kcal/mol. [e] Population based on Gibbs energies.

TABLE 2: Comparison of Predicted and Observed Frequencies and Vibrational Assignments for (2*R*,3*R*)-2,3-Butanediol

band no.[a]	exp. (cm^{-1})[b]	pred. (cm^{-1})[c,d]	cal. (cm^{-1})[c,e]	assignment[f]
ν_1	1453	1464	1523	CH_3 deformation
ν_2	1446	1455	1516	CH_3 deformation
ν_3	1398	1404	1461	CH_3 deformation
ν_4	1377	1386	1442	CH_3 deformation, CH and COH wag
ν_5		1374	1429	CH_3 deformation, CH and COH wag
ν_6	1308	1312	1365	CH wag and COH A,B bend
ν_7	1262	1281	1333	COH A,B bend, CH wag
ν_8	1243*	1263	1314	COH A,B bend, CH wag
ν_9	1229*	1243	1293	COH A,B bend, CH wag
ν_{10}	1217*	1216	1265	COH B bend, CH wag
ν_{11}	1177	1172	1219	COH A,B bend, CH wag
ν_{12}	1151	1137	1183	C−O B,A stretch, CH_3 wag
ν_{13}	1125	1128	1173	C−O A stretch, CH_3 wag
ν_{14}	1103*	1103	1147	COH A bend, CH_3 wag
ν_{15}	1099	1081	1125	C−O B stretch, COH A,B bend, and CH_3 wag
ν_{16}	1094*	1075*	1116*	C−O B stretch, COH A,B bend, and CH_3 wag
ν_{17}	1072	1057	1100	CH_3 wag, C−O B stretch and COH A,B bend
ν_{18}		1044	1086	CH_3 wag, COH B bend
ν_{19}	1046	1026	1067	COH A,B bend, CH_3 wag and C−O A,B stretch
ν_{20}	1010*	984*	1025*	CH_3 wag, CH wag
ν_{21}	992	980	1019	C−O A,B stretch, CH_3 wag
ν_{22}	965	949	987	CH_3 wag, CH wag
ν_{23}	929	910	947	CH_3 wag, C−C stretch
ν_{24}	891	873	908	CH_3 wag, C−C stretch

[a] These numbers derived from Pred. 1 in Figure 2. [b] Experimental wavenumbers obtained from the absorption spectrum at concentrations of 0.01 and 0.077 M; asterisks (*) denote the bands that show as shoulders in the spectrum. [c] Band positions from the simulated spectra with populations given in Table 1; asterisks (*) denote the bands that show as shoulders in the spectrum. [d] Ab initio wavenumbers scaled with 0.96; asterisks (*) denote the bands that show as shoulders in the spectrum. [e] Unscaled ab initio wavenumbers. [f] Based on vibrational analysis and verified by the results deduced from Gaussview (version 2.1); "A" and "B" denote the COH group of type A and type B (see Figure 1), respectively, in the formation of intramolecular hydrogen bond.

most stable conformation is that labeled as ($g^-G^-g'^+$) or equivalent conformation ($g^+G^-g'^-$).

All of the 10 unique low energy conformers investigated are found to have energy minima (all vibrational frequencies are real) at the B3LYP/6-31G* level, so the absorption and VCD intensities have been calculated for all of them at the B3LYP/6-31G* level. In Table 2, the calculated frequencies come from the population-weighted theoretical spectra and the observed bands are assigned to the six lowest energy unique conformers, namely, ($g^-G^-g'^+$), ($tG^-g'^+$), (g^-G^+t'), ($g^+G^-g'^+$), ($g^-G^+g'^+$), and ($g^-G^+g'^-$). The predicted absorption and VCD spectra simulated with 8 cm^{-1} half-widths and Lorentzian band shapes are shown in Figures 2 and 3. The vibrational frequencies obtained in B3LYP/6-31G* calculation have been multiplied

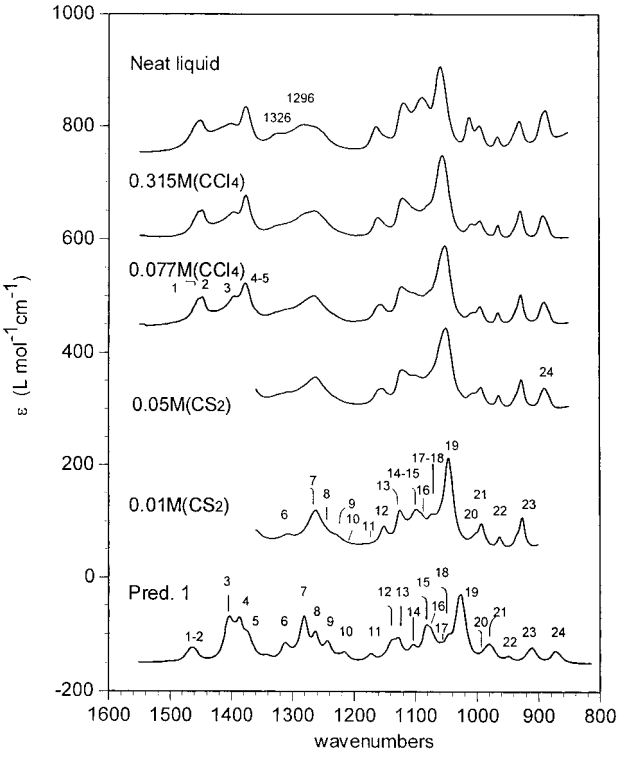

Figure 4. Comparison of the experimental absorption spectra of (2*R*,3*R*)-(−)-2,3-butanediol at different concentrations (top five traces) with the predicted (population-weighted) absorption (bottom trace) obtained with the B3LYP/6-31G* basis set. The spectra were simulated with Lorentzian band shapes and 8 cm^{-1} half-widths, and frequencies were multiplied with 0.96. The labels on the top five traces give concentration employed for the experimental spectra. The labels for the peaks are the same as those in Table 2.

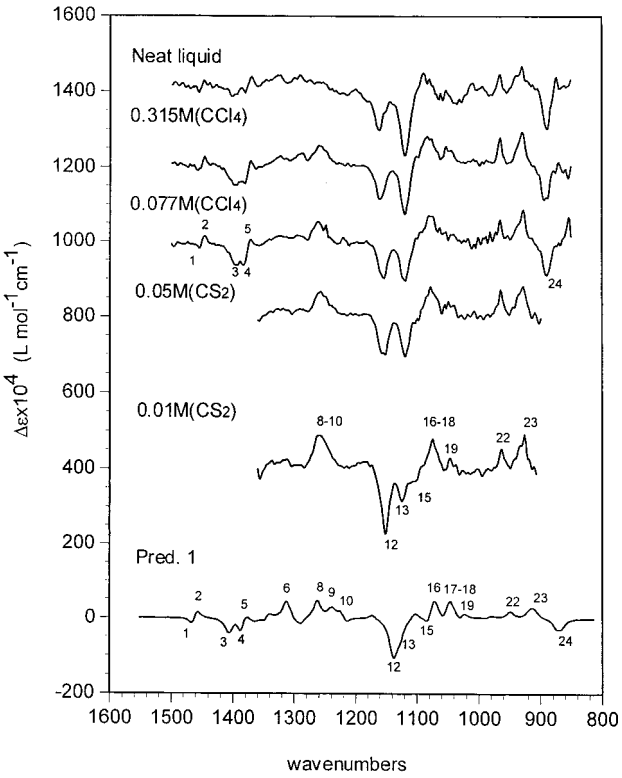

Figure 5. Comparison of the experimental VCD spectra of (2*R*,3*R*)-(−)-2,3-butanediol at different concentrations (top five traces) with the VCD predicted (population-weighted) for (2*R*,3*R*)-2,3-butanediol (bottom trace) using the B3LYP/6-31G* basis set. The spectra were simulated with Lorentzian band shapes and 8 cm^{-1} half-widths, and frequencies were multiplied with 0.96. The labels on the top five traces give concentration employed for the experimental spectra. The labels for the peaks are the same as those in Table 2.

by 0.96. These theoretical spectra can be compared (Figures 4 and 5) to the experimental spectra of (2*R*,3*R*)-(−)-2,3-butanediol at different concentrations. The predicted frequencies for isolated molecule match the observed frequencies of (2*R*,3*R*)-2,3-butanediol well at low concentration (see Table 2 and Figure 4), except that (a) bands corresponding to 1281 (#7), 1263 (#8), 1243 (#9), and 1216 (#10) cm^{-1} in the predicted absorption spectrum do not appear as resolved in the experimental spectrum, (b) bands at 1151 (#12) and 1125 (#13) cm^{-1} in the experimental absorption spectrum are clearly separated, but the corresponding bands are closely positioned in predicted absorption spectrum, and (c) the experimental bands corresponding to the predicated bands at 1386 (#4) and 1374 (#5) cm^{-1}, at 1103 (#14), 1081 (#15) and 1075 (#16) cm^{-1}, and at 1057 (#17) and 1044 (#18) cm^{-1} are not resolved in the experimental absorption spectra.

The experimental absorption spectrum at lower concentration contains 22 bands at ∼1453, 1446, 1398, 1377, 1308, 1262, 1243 (shoulder), 1229(shoulder), 1217 (shoulder), 1177 (small), 1151, 1125, 1103 (shoulder), 1099, 1094 (shoulder), 1072, 1046, 1010 (shoulder), 992, 965, 929, and 891 cm^{-1} in the 1500−890 cm^{-1} region. As concentration increases, the bands at 1046 (#19), 1072 (#17 and 18), 1099 (#15), 1094 (#16), and 1151 (#12) cm^{-1} shift to higher frequencies and become broadened, and the bands at 1262 (#7) and 1308 (#6) cm^{-1} shift to 1296 and 1326 cm^{-1}, respectively. However, the band at 1125 (#13) remains at the same position. From Table 2, of the bands assigned to CO stretching or COH bending vibration, the bands at 1125 (#13) and 1103 (#14) come from the COH group of type A (see $C_1O_2H_A$ in Figure 1) that is locked in intramolecular hydrogen bond, which is not largely influenced by the formation of intermolecular hydrogen bonding, while the other bands are at least partly attributed to the COH group of type B (see $C_4O_6H_B$ in Figure 1) that is free to donate hydrogen in the formation of intermolecular hydrogen bond. The intermolecular hydrogen bonding makes C−O−H bending and C−O stretching vibrations from COH group of type B shift to higher frequencies due to the changes in force constants upon hydrogen bonding.[18] In addition, as the concentration is increased, the relative intensities of bands at 1010 (#20) and 992 (#21) cm^{-1} are reversed for neat liquid. This is probably because the 992 cm^{-1} band (which is assigned to C−O stretch vibration) is shifted to higher frequencies due to intermolecular hydrogen bonding and overlaps with the 1010 cm^{-1} band at higher concentrations. However, a significant decrease in intensity of the band at 992 cm^{-1} is not seen, which may be due to the fact that this band is attributed to C−O stretch from the COH groups of both type A and type B and also to CH_3 wag. At lower concentrations, intermolecular hydrogen bonding is expected to be less significant, so the experimental spectra at lower concentrations are expected to be closer to those predicted for isolated molecules. This in fact is evident in Figure 4, where the population-weighted theoretical absorption spectrum compares more favorably to the experimental absorption spectrum obtained at 0.01 M (CS_2) concentration. Nevertheless, the intermolecular hydrogen bonding is still evident even in dilute solution because the bands at 1103 (#14), 1081 (#15), and 1075 (#16) cm^{-1} (which are attributed to CO stretch or COH bend vibration) in the predicted spectrum appear as one overlapping band centered at 1099 (#14−16) in dilute solution. The bands in dilute solution, corresponding to 1312 (#6), 1281 (#7), 1263 (#8), 1243 (#9),

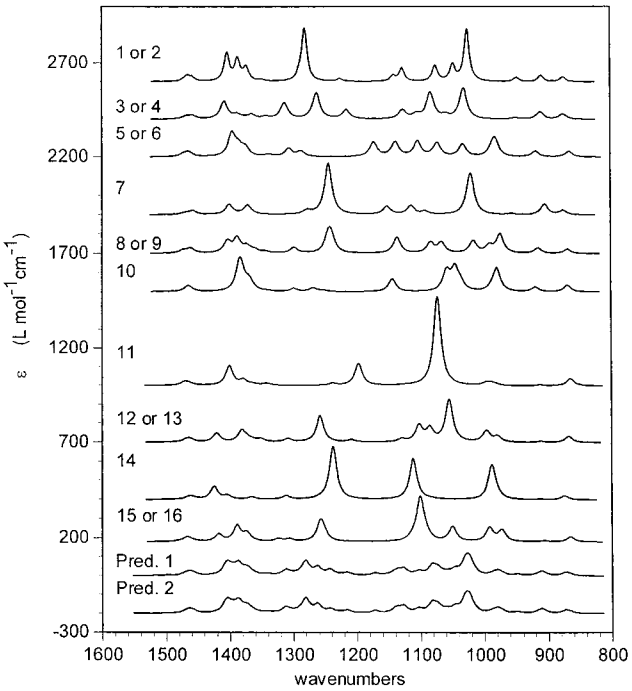

Figure 2. Ab initio vibrational absorption spectra for sixteen conformers of (2*R*,3*R*)-(−)-2,3-butanediol obtained with the B3LYP/6-31G* basis set. The spectra were simulated with Lorentzian band shapes and 8 cm^{-1} half-widths, and frequencies were multiplied with 0.96. The labels on the traces are the conformation labels (Figure 1). The predicted absorption spectra are obtained by adding the population-weighted absorption spectra of all conformers. The populations used to obtain Pred. 1 and Pred. 2 are those expected for isolated molecules (Table 1) and molecules in self-consistent reaction field (Table 3), respectively.

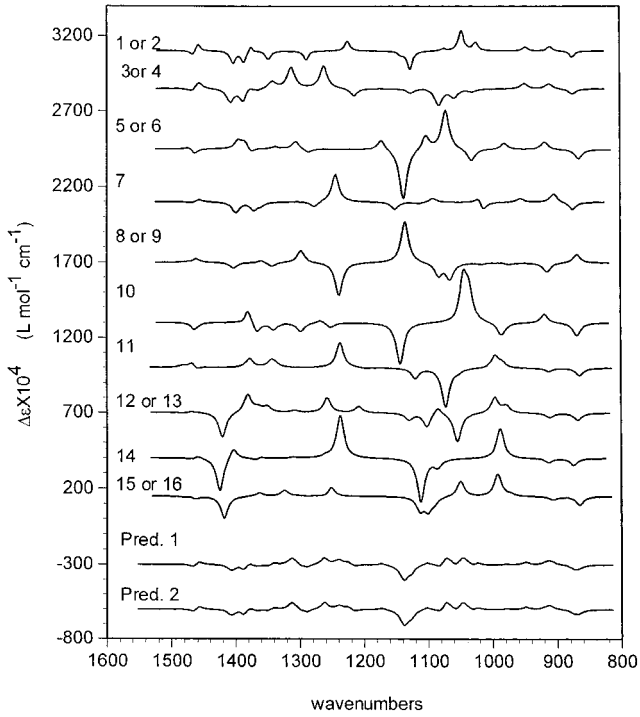

Figure 3. Ab initio VCD spectra for 16 conformers of (2*R*,3*R*)-(−)-2,3-butanediol obtained with the B3LYP/6-31G* basis set. The spectra were simulated with Lorentzian band shapes and 8 cm^{-1} half-widths, and frequencies were multiplied with 0.96. The labels on the traces are the conformation labels (Figure 1). The predicted VCD spectra are obtained by adding the population-weighted VCD spectra of all conformers. The populations used to obtain Pred. 1 and Pred. 2 are those expected for isolated molecules (Table 1) and molecules in self-consistent reaction field (Table 3), respectively.

and 1216 (#10) cm^{-1} bands in the predicted spectrum, appear as broad or overlap each other in the experimental spectrum and also indicate the existence of intermolecular hydrogen bonds in dilute solution. In addition, the bands at 1151 (#12) and 1125 (#13) cm^{-1} are well resolved in dilute solution. From Table 2, the band at 1151 (#12) cm^{-1} comes partly from CO stretch of the COH group of type B, while the band at 1125 (#13) cm^{-1} is attributed to CO stretch of the COH group of type A. Then during the formation of the intermolecular hydrogen bonds, the CO stretch of the COH group of type B(#12) shifts to higher frequency, and the CO stretch (#13) of the COH group of type A remains at the same position, which makes the two bands separated more from each other as the concentration increases. The presence of some separation even in dilute solution and the very little separation in the predicated spectrum suggest that there is some amount of intermolecular hydrogen bonding even in dilute solutions. There are not considerable differences in relative intensities of the bands at 1453 (#1), 1446 (#2), 1398 (#3), 1377 (#4−5) cm^{-1} and at 965 (#22), 929 (#23), and 891 (#24) cm^{-1} with the increase of concentration, which indicates that there are not significant differences in conformational populations at different concentrations because these bands should be sensitive to the change in populations of conformations (see Figure 2).

In Table 3, the populations predicted for molecules in dilute solution on the basis of the calculation with self-consistent reaction field (SCRF) methods[19] show only minor differences from those predicted for isolated molecules. In comparing Tables 1 and 3, note that for degenerate pairs of conformers only one conformation for each pair is listed in Table 3. Then the population difference obtained in solvent reaction field would have no significant influence on the population-weighted theoretical absorption and VCD spectra (shown in Figures 2 and 3).

The experimental VCD spectra (Figure 5) at concentration of 0.01 M(CS_2) and 0.077(CCl_4) show 14 bands at 1455 (−), 1446 (+), 1397 (−), 1380 (−), 1371 (+), 1261 (+), 1150 (−), 1124 (−), 1100 (−), 1073 (+), 1046 (+), 962 (+), 927 (+), and 890 (−) cm^{-1}. As the concentration is increased, the intensities of positive VCD bands centered at 1261 (#8−10) and 1073 (#16−18) cm^{-1} shift to higher frequencies and become broad, the relative intensities for the bands at 1150 (#12) and 1124 (#13) cm^{-1} are reversed, and the bands at 1150 (#12), 1099 (#15), 1073 (#16−18), and 1046 (#19) shift to higher frequencies. These bands are attributed to at least partly to C−O−H bending or C−O stretch vibrations from the COH group of type B (free to donate hydrogen in the formation of intermolecular hydrogen bond); therefore, the results indicate the influence of intermolecular hydrogen bonding on free COH bending and C−O stretch vibrations. The population-weighted theoretical VCD spectrum obtained for (2*R*,3*R*)-configuration matches better with the experimental VCD spectrum of (−)-2,3-butanediol obtained at 0.01 M concentration.

The differences between predicted and experimental (0.01 M) VCD spectra might be attributed to the intermolecular hydrogen bonding effect that is present even at dilute concentrations. The bands at 1262 (#8), 1242 (#9), and 1216 (#10) cm^{-1} in the predicted spectrum appear as only one band at 1261 cm^{-1} in dilute solution; the bands corresponding to 1075 (#16), 1057 (#17), and 1044 (#18) cm^{-1} in predicted spectrum are not resolved in experimental spectrum. The intensities of bands at 1455 (#1), 1446 (#2), 1397 (#3), 1380 (#4), 1371 (#5), 962

TABLE 3: Influence of Self-consistent Reaction Field (SCRF)[19] on Conformational Stability

			isolated molecule		molecule in SCRF	
labels[a]	dipole moment[b]	radius[c] (Å)	gibbs[d]	pop.[e]	Gibbs[d]	pop.[e]
1 ($g^-G^-g'^+$)	2.4926	3.95	−308.768698	0.169	−308.769343	0.178
3 ($tG^-g'^+$)	2.6598	4.07	−308.768535	0.142	−308.769179	0.150
5 (g^-G^+t')	2.4744	3.94	−308.768015	0.082	−308.768663	0.087
7 ($g^+G^-g'^+$)	0.4384	3.74	−308.767673	0.057	−308.767120	0.017
8 ($g^-G^+g'^+$)	2.3513	3.94	−308.767571	0.051	−308.768182	0.052
10 ($g^-G^+g'^-$)	0.2588	4.10	−308.767544	0.050	−308.768058	0.046
11 (tTt')	0.3084	4.06	−308.763949	0.001	−308.764041	0.001
12 (g^+Tt')	2.0844	3.66	−308.763781	0.001	−308.764400	0.001
14 ($g^+Tg'^+$)	1.9978	3.86	−308.763655	0.001	−308.764138	0.001
15 ($g^-Tg'^+$)	0.3764	4.02	−308.763651	0.001	−308.763737	0.001

[a] See Figure 1 for the labels. [b] In Debye. [c] Radius a_0 of spherical cavity for solute. [d] In Hartrees. [e] Population based on Gibbs energies. For degenerate pairs of conformers, only one conformer for each pair is listed here. See Table 1 for complete list.

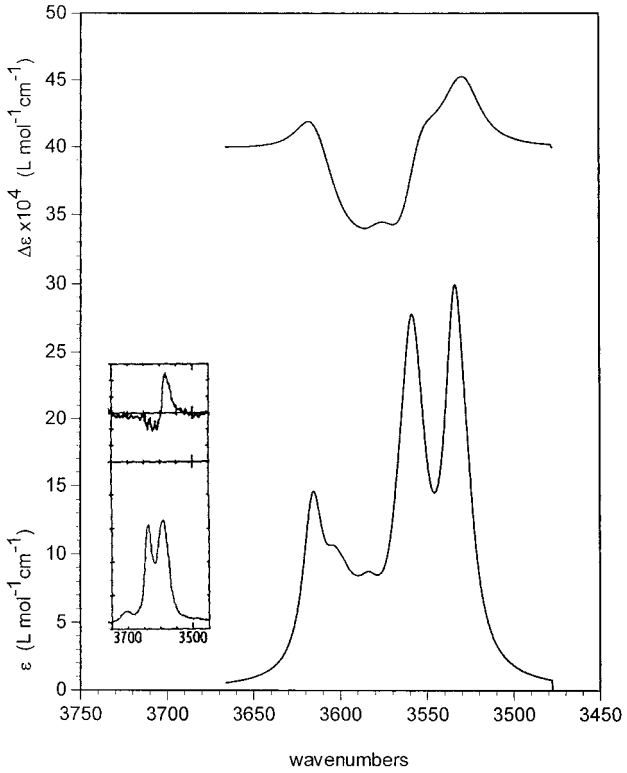

Figure 6. Comparison of absorption and VCD spectra of (2*R*,3*R*)-(−)-2,3-butanediol in the OH stretching region. The predicted absorption and VCD spectra were obtained with the B3LYP/6-31G* basis set. The spectra were simulated with Lorentzian band shapes and 8 cm^{-1} half-widths, and frequencies were multiplied with 0.96. They were obtained by adding the population-weighted absorption and VCD spectra of all conformers. The experimental absorption and VCD spectra in the inset are reproduced from Yamamoto, K.; et al. Vibrational Circular Dichroism in Hydrogen Bonded Systems. *J. Mol. Struct.* **1991**, *242*, 75−86.

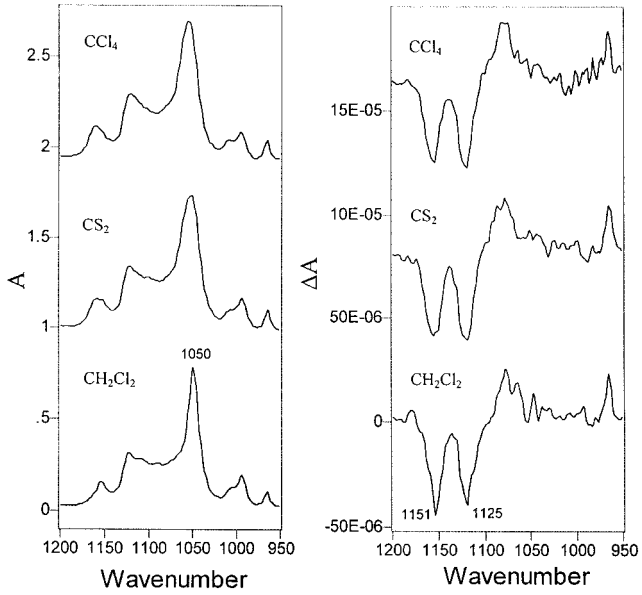

Figure 7. Comparison of the experimental absorption and VCD spectra of (−)-2,3-butanediol (∼0.05 M) in CH_2Cl_2, CS_2, and CCl_4 solutions. The labels on the experimental traces give solvent employed for the experimental spectra.

(#22), 927 (#23), and 890 (#24) cm^{-1} remain almost the same at 0.077 and 0.315 M, indicating that intermolecular hydrogen bonding may not have a significant influence on the composition of the conformations for chiral (2*R*,3*R*)-(−)-2,3-butanediol in solution phase.

In Figure 6, the predicted absorption and VCD spectra in O−H stretching region are shown. The VCD spectra in this region were reported by by Sugeta et al.[4b] for (−)-2,3-butanediol in dilute CCl_4 solution. Their experimental spectra are reproduced in Figure 6 for comparison to our predicted spectra. These experimental spectra are in qualitative agreement with the predicted spectra. There are two strong absorption bands in both experimental and predicted spectra, with approximately the same relative intensities. These two absorption bands are associated with negative−positive VCD (negative VCD on the higher frequency side), both in experimental and predicted spectra. Nevertheless, comparison of experimental spectra with predicted spectra in the O−H stretching region cannot be done quantitatively, since anharmonic effects play a significant role in this region. Such effects, although unavoidable in the experimental spectra, are not included in the predicted spectra.

The solvent influence on the absorption and VCD spectra is shown in Figure 7. As the solvent changes from nonpolar (CCl_4 and CS_2) to polar (CH_2Cl_2), the broad absorption band at ∼1050 cm^{-1} becomes narrow. Similarly in the VCD spectrum, the relative intensities of the bands at 1151 and 1125 cm^{-1} are seen to be reversed as the solvent changes from nonpolar to polar. The more polar the solvent is, the stronger the interactions with solvent will be, resulting in fewer intermolecularly hydrogen bonded dimers and trimers. Such solute−solvent interactions can account for the narrowing of absorption band at 1050 cm^{-1} in CH_2Cl_2.

Thus, on the basis of the absorption and VCD spectra obtained at different concentrations and solvents and the corresponding theoretical spectra, it appears that the relative populations predicted for isolated (2*R*,3*R*)-(−)-2,3-butanediol are applicable to the solution phase sample at lower concentrations. At higher concentrations, because of the influence of intermolecular

hydrogen bonding on free C−O−H bending and C−O stretching, there are corresponding shifts in the vibrational absorption and VCD spectra. Conformational composition does not appear to change with concentration for (2*R*,3*R*)-(−)-2,3-butanediol, which is supported by small differences in dipole moments of the predominant conformations. It is evident that polarity of solvent also has an influence on the existence of intermolecular hydrogen bonding.

Summary

The comparison of experimental and ab initio predicted absorption and VCD spectra indicate the following: (a) (−)-2,3-butanediol is of (2*R*,3*R*) configuration; (b) the Gibbs energies of different conformations are closely spaced and 10 predominant conformations of (2*R*,3*R*)-(−)-2,3-butanediol (conformers 1−10 in Table 1) are present at low concentrations in nonpolar solvents; (c) gauche O−C−C−O conformations (G^-) and (G^+) are more stable than trans (T) conformations, and the most stable conformation is ($g^+G^-g'^-$); (d) intermolecular hydrogen bonding makes the bands assigned to free C−O−H bending and C−O stretching shift to higher frequencies, but its influence on the conformational composition of chiral (2*R*,3*R*)-(−)-2,3-butanediol is small; (e) the intermolecular hydrogen bonding is clearly evident in nonpolar solvents.

Acknowledgment. Grants from NSF (CHE9707773) and Vanderbilt University are gratefully acknowledged.

References and Notes

(1) (a) Grochowski, J.; Rys, B.; Serda, P.; Wagner, U. *Tetrahdron: Asymmetry* **1995**, *6*, 2059. (b) Davies, S. G.; Newton, R. F.; Williams, J. M. J. *Tetrahedron Lett*. **1989**, *30*, 2967. (c) Angiolini, L.; Carlini, C.; Salatelli, E. *Makromol. Chem*. **1992**, *193*, 2883. (d) Awano, K.; Yanai, T.; Watanabe, I.; Takagi, Y.; Kitahara, T.; Mori, K. *Biosci. Biotechnol. Biochem.* **1995**, *59*, 1251.

(2) Plattner, J. J.; Rapoport, H. *J. Am. Chem. Soc*. **1971**, *93*, 1758.

(3) Szarecka, A.; Hoffmann, M.; Rychlewski, J.; Rychlewska, U. *J. Mol. Struct*. **1996**, *374*, 363.

(4) (a) Gallwey, F. B.; Hawkes, J. E.; Haycock, P.; Lewis, D. *J. Chem. Soc., Perkin. Trans. 2* **1990**, *11*, 1979. (b) Yamamoto, K.; Nakao, Y.; Kyogoku, Y.; Sugeta, H. *J. Mol. Struct*. **1991**, *242*, 75.

(5) (a) Schneider, H. J.; Lonsdorfer, M. *Org. Magn. Reson*. **1981**, *16*, 133. (b) Levy, G. C.; Pehk, T.; Lippmaa, E. *Org. Magn. Reson*. **1980**, *14*, 214.

(6) Duin, M. V.; Baas, J. M. A.; Graaf, B. V. D. *J. Org. Chem*. **1986**, *51*, 1298.

(7) Polavarapu, P. L.; Zhao, C.; Ramig, K. *Tetrahedron: Asymmetry* **1999**, *10*, 1099. Polavarapu, P. L.; Cholli, A.; Vernice, G. *J. Am. Chem. Soc.* **1992**, *114*, 10953. Polavarapu, P. L.; Zhao, C.; Cholli, A. L.; Vernice, G. *J. Phys. Chem. B* **1999**, *103*, 6127.

(8) Costante, J.; Hecht, L.; Polavarapu, P. L.; Collet, A.; Barron, L. D. *Angew. Chem., Int. Ed. Engl*. **1997**, *36*, 885. Ashvar, C. S.; Devlin, F. J.; Stephens, P. J. *J. Am. Chem. Soc*. **1999**, *121*, 2836.

(9) Becke, A. D. *J. Chem. Phys*. **1993**, *98*, 1372, 5648.

(10) Cheeseman, J. R.; Frisch, M. J.; Devlin, F. J.; Stephens, P. J. *Chem. Phys. Lett.* **1996**, *252*, 211.

(11) Frisch, M. J.; Trucks, G. W.; Schlegel, H. B.; Scuseria, G. E.; Robb, M. A.; Cheeseman, J. R.; Zakrzewski, V. G.; Montgomery, J. A., Jr.; Stratmann, R. E.; Burant, J. C.; Dapprich, S.; Millam, J. M.; Daniels, A. D.; Kudin, K. N.; Strain, M. C.; Farkas, O.; Tomasi, J.; Barone, V.; Cossi, M.; Cammi, R.; Mennucci, B.; Pomelli, C.; Adamo, C.; Clifford, S.; Ochterski, J.; Petersson, G. A.; Ayala, P. Y.; Cui, Q.; Morokuma, K.; Malick, D. K.; Rabuck, A. D.; Raghavachari, K.; Foresman, J. B.; Cioslowski, J.; Ortiz, J. V.; Stefanov, B. B.; Liu, G.; Liashenko, A.; Piskorz, P.; Komaromi, I.; Gomperts, R.; Martin, R. L.; Fox, D. J.; Keith, T.; Al-Laham, M. A.; Peng, C. Y.; Nanayakkara, A.; Gonzalez, C.; Challacombe, M.; Gill, P. M. W.; Johnson, B.; Chen, W.; Wong, M. W.; Andres, J. L.; Gonzalez, C.; Head-Gordon, M.; Replogle, E. S.; Pople, J. A. *Gaussian 98*, revision A.3; Gaussian, Inc.: Pittsburgh, PA, 1998.

(12) Barron, L. D. *Tetrahedron* **1978**, *34*, 607.

(13) (a) Wang, F.; Polavarapu, P. L. *J. Phys. Chem. A* **2000**, *104*, 10683. (b) Wang, F.; Polavarapu, P. L. *J. Phys. Chem. A* **2000**, *104*, 1822.

(14) Wang, F.; Polavarapu, P. L. *J. Phys. Chem. A* **2000**, *104*, 6189.

(15) A. D. Becke *Phys. Rev. A* **1988** *38*, 3098.

(16) Hehre, W. J.; Radom, L.; Schleyer, P. V. R.; Pople, J. A. *Ab initio Molecular Orbital Theory*; John Wiley & Sons: New York, 1986.

(17) Schachtschneider, J. H. *Vibrational Analysis of Polyatomic Molecules*; Reports 231/64 and 57/65; Shell Development Co.: Houston, TX, 1962.

(18) Sun, Z.; Wang, F.; Tang, Z.; Yan, G. *Chin. J. Atom. Mol. Phys.* **1995**, *12*, 375. Lozynski, M.; Roszak, D. R.; Mack, H.-G. *J. Phys. Chem. A* **1998**, *102*, 2899.

(19) Wong, M. W.; Frisch, M. J.; Wiberg, K. B. *J. Am. Chem. Soc*. **1991**, *113*, 4776.